On the Equivalence of Dual-Wavelength and Dual-Polarization Equations for Estimation of the Raindrop Size Distribution

ROBERT MENEGHINI

NASA GSFC, Greenbelt, Maryland

LIANG LIAO

Goddard Earth Sciences and Technology Center/Caelum Research Corp., Rockville, Maryland

(Manuscript received 4 May 2006, in final form 21 August 2006)

ABSTRACT

For air- and spaceborne weather radars, which typically operate at frequencies of 10 GHz and above, attenuation correction is usually an essential part of any rain estimation procedure. For ground-based radars, where the maximum range within the precipitation is usually much greater than that from air- or spaceborne radars, attenuation correction becomes increasingly important at frequencies above about 5 GHz. Although dual-polarization radar algorithms rely on the correlation between raindrop shape and size, while dual-wavelength weather radar algorithms rely primarily on non-Rayleigh scattering at the shorter wavelength, the equations for estimating parameters of the drop size distribution (DSD) are nearly identical in the presence of attenuation. Many of the attenuation correction methods that have been proposed can be classified as one of two types: those that employ a kZ (specific attenuation–radar reflectivity factor) relation, and those that use an integral equation formalism where the attenuation is obtained from the DSD parameters at prior gates, either stepping outward from the radar or inward toward the radar from some final range gate. The similarity is shown between the dual-polarization and dual-wavelength equations when either the kZ or the integral equation formulation is used. Differences between the two attenuation correction procedures are illustrated for simulated measurements from an X-band dual-polarization radar.

1. Introduction

The close connection between dual-polarization and dual-wavelength radar algorithms can be understood from similarities in the two sets of measurements. Typically, two parameters of the hydrometeor size distribution are estimated from two independent radar reflectivity factor measurements. In the dual-polarization case, the independent data are the copolarized radar reflectivity factors at horizontal and vertical polarizations. The dual-wavelength radar provides radar reflectivity factors at two wavelengths at the same polarization state.

A further similarity between the two situations is that the measured or apparent reflectivity factors must be corrected for attenuation before the estimation of the size distribution parameters can be made. The attenuation correction can proceed either in the forward direction, with increasing radar range, or in the backward direction, starting from a final gate and progressing inward toward the radar. However, the forward-going solutions tend to be unstable because the attenuation out to the range of interest becomes "large" in some sense. This is analogous to the case of a single attenuating-wavelength radar where the forward solution to the Hitschfeld–Bordan (Hitschfeld and Bordan 1954) equation becomes unstable as the attenuation increases. To circumvent this problem, the equations can be expressed in a form that includes an independent estimate of path attenuation. For the dual-polarization radar, it has been shown that a measurement of the differential phase between horizontal and vertical polarizations (Testud et al. 2000; Bringi et al. 2001; Matrosov et al. 2002, 2005) provides a good estimate of path attenuation at the two polarizations. For airborne and spaceborne dual-wavelength measurements, the surface ref-

Corresponding author address: Robert Meneghini, Code 614.6, Instrumentation Sciences Branch, NASA Goddard Space Flight Center, Greenbelt, MD 20771.
E-mail: bob@neptune.gsfc.nasa.gov

DOI: 10.1175/JTECH2005.1

erence technique can be used to estimate path attenuation at both wavelengths.

In this paper, two types of attenuation correction procedures are formulated for application to dual-wavelength and dual-polarization weather radar data. In the integral equation approach, which has been used in the analysis of dual-wavelength airborne radar data, the parameters of the drop size distribution (DSD) are used to adjust the path attenuation to the adjacent range gate, which, in turn, is used to correct the measured reflectivity factors at that gate. In this way, a recursion procedure is defined. The most notable use of the kZ (specific attenuation–radar reflectivity factor) parameterization approach was provided by Hitschfeld and Bordan (1954) who analyzed the radar equation for a single attenuating-wavelength radar. Modification of this estimate to include an independent path attenuation constraint has led to its application in the analysis of airborne and spaceborne radar data. An important recent development is the application of methods of this type to polarimetric data. The approach has not, however, been widely used for the analysis of dual-wavelength radar data.

The primary objective of the paper is to make clear the relationships between the polarimetric and dual-wavelength equations in the presence of attenuation for both the integral equation and kZ parameterization approaches. We begin by writing the integral equations for the median mass diameter D_0 and number concentration N_t that are applicable to both dual-polarization and dual-wavelength radar returns for the initial value and final value cases. This is followed by a similar development for the kZ parameterization. For this case, however, only the final value version is discussed. Simulations of the retrievals are presented for the case of an X-band polarimetric radar with an emphasis on the differences between the backward solutions using the integral equation and kZ parameterization.

2. Integral equations

The integral equations can be written in a relatively simple form, but at the expense of requiring several definitions. The measured radar reflectivity factor at range r and frequency f, $Z_{m,pp}(r, f)$ (mm^{6}m^{-3}), when the transmit and receive polarization are along the direction p, can be defined in terms of the radar return power $P_{r,pp}(r, f)$ by

$$Z_{m,pp}(r,f) = P_{r,pp}(r,f)r^2/[C_{pp}(f)|K_w(f)|^2], \qquad (1)$$

where C is the radar constant and $|K_w|^2$ is the dielectric factor of water, which, by the convention used here, is taken to be equal to its approximate value (0.93) for frequencies between 3 and 10 GHz and for temperatures between 0° and 20°C (Battan 1973). The nonattenuated effective radar reflectivity factor, or simply radar reflectivity factor Z, is related to Z_m by

$$Z_{pp}(r,f) = Z_{m,pp}(r,f) \times \exp\left\{c\int_0^r [k_{r,pp}(s,f) + k_c(s,f) + k_v(s,f)]\,ds\right\}, \qquad (2)$$

where k_r, k_c, and k_v are the specific attenuations from precipitation, cloud water, and water vapor, respectively, and where the precipitation may include rain, snow, and mixed-phase hydrometeors. Throughout the paper, the copolarized return powers are denoted by the subscripts pp, where the first subscript represents the polarization state of the transmitted wave and the second the polarization state of the received signal. Because only horizontal h and vertical v copolarized signals are considered, pp is equal either to hh or vv. Because the cloud and water vapor attenuation are polarization independently, we omit subscripts on these quantities. The units of k are taken to be decibels per kilometer so that $c = 0.2\ \ln(10) = 0.46$. To further simplify the equations, we let

$$\tilde{Z}_{m,pp}(r,f) = 10\log Z_{m,pp}(r,f),$$
$$\tilde{Z}_{pp}(r,f) = 10\log Z_{pp}(r,f), \qquad (3)$$

where the logarithms in (3) and throughout the paper are taken to base 10. Using (3), (2) can be written as

$$\tilde{Z}_{m,pp}(r,f) = \tilde{Z}_{pp}(r,f) - A_{pp}(0,r;f) = \tilde{Z}_{pp}(r,f) - [A_{pp}(0,r_n;f) - A_{pp}(r,r_n;f)], \qquad (4)$$

where the two-way path attenuation from r_1 to r_2 is

$$A_{pp}(r_1,r_2;f) = 2\int_{r_1}^{r_2} [k_{r,pp}(s,f) + k_c(s,f) + k_v(s,f)]\,ds \equiv A_{r,pp}(r_1,r_2;f) + A_c(r_1,r_2;f) + A_v(r_1,r_2;f). \qquad (5)$$

In the equations below, the notation $A_{pp}(0, r; f) = A_{pp}(r, f)$ is used. It should be noted that the nth gate, at range r_n, is taken as the final gate of the path so that the total path-integrated attenuation (PIA) is $A_{pp}(r_n, f)$. Next, the raindrop diameter distribution $N(D, s)$ (m^{-3} mm^{-1}) is expressed as the product of the particle number concentration N_t (m^{-3}), and a normalized size distribution $n(D)$ (mm^{-1}),

$$N(D) = N_t n(D), \tag{6}$$

where, for the gamma distribution,

$$n(D; \mu, \Lambda) = [\Lambda^{(\mu+1)} D^{\mu}/\Gamma(\mu + 1)] \exp[-\Lambda D]. \tag{7}$$

In general, Λ, μ are functions of the radar range. In the numerical results presented later, we use the median mass diameter D_0 (mm), related to Λ, μ, by (Ulbrich 1983)

$$\Lambda D_0 = 3.67 + \mu. \tag{8}$$

Finally, we introduce backscattering and extinction integrals that are independent of N_t:

$$I_{b,pp}(r, f; D_0, \mu) = 10 \log\left[c_Z \int_0^{\infty} \sigma_{b,pp}(f, D) n(r, D; D_0, \mu)\, dD\right], \tag{9}$$

$$I_{e,pp}(r, f; D_0, \mu) = c_e \int_0^{\infty} \sigma_{e,pp}(f, D) n(r, D; D_0, \mu)\, dD, \tag{10}$$

where $c_Z = c_0^4/(f^4 \pi^5 |K_w|^2)$ and $c_e = 4.343 \times 10^{-3}$, and where c_0 is the speed of light. Note that $k_{r,pp} = N_t I_{e,pp}$ and $\tilde{Z}_{pp} = I_{b,pp} + 10 \log N_t$.

Integral equations for D_0 and N_t for the dual-polarization case can be obtained by writing $\tilde{Z}_{m,pp}(r, f)$ and $\tilde{Z}_{m,\mathrm{hh}}(r, f) - \tilde{Z}_{m,\mathrm{vv}}(r, f)$ in terms of D_0 and N_t and expressing the path attenuation to range r in the form (Meneghini et al. 1992)

$$\begin{aligned} A_{pp}(r, f) &= A_{pp}(r_n, f) - A_{pp}(r, r_n; f) \\ &= A_{pp}(r_n, f) - 2\int_r^{r_n} N_t(s) I_{e,pp}(s)\, ds. \end{aligned} \tag{11}$$

In (11), the attenuation from r to r_n is written in terms of the DSD parameters at the range gates within this range interval. This is the essence of the backward integral equation approach, where path attenuation to range r is found from an estimate of the total path attenuation and the DSD parameters in the range from r to r_n. The equations can be written in the form

$$I_{b,\mathrm{hh}}(r) - I_{b,\mathrm{vv}}(r) = [\tilde{Z}_{m,\mathrm{hh}}(r) - \tilde{Z}_{m,\mathrm{vv}}(r)] + [A_{\mathrm{hh}}(r_n) - A_{\mathrm{vv}}(r_n)] - 2\int_r^{r_n} N_t(s)[I_{e,\mathrm{hh}}(s) - I_{e,\mathrm{vv}}(s)]\, ds, \tag{12}$$

$$\tilde{N}_t(r) = \tilde{Z}_m(r) - I_b(r) + A_r(r_n) - 2\int_r^{r_n} N_t(s) I_e(s)\, ds + A_c(r) + A_v(r), \tag{13}$$

where

$$\tilde{N}_t \equiv 10 \log_{10} N_t. \tag{14}$$

For the dual-wavelength case, (13) remains the same but (12) is modified to

$$\begin{aligned} I_b(r, f_1) - I_b(r, f_2) = {} & [\tilde{Z}_m(r, f_1) - \tilde{Z}_m(r, f_2)] + [A_r(r_n, f_1) - A_r(r_n, f_2)] - 2\int_r^{r_n} N_t(s)[I_e(s, f_1) - I_e(s, f_2)]\, ds + [A_c(r, f_1) \\ & - A_c(r, f_2)] + [A_v(r, f_1) - A_v(r, f_2)]. \end{aligned} \tag{15}$$

Note that the last four terms on the right-hand side of (15) are absent in (12). The difference arises from the fact that cloud and water vapor attenuation are frequency dependent but polarization independent. We have used the convention of suppressing the polarization (or frequency) dependence if all quantities in the equation are at the same polarization (or frequency). For example, in (12) all quantities are at the same frequency, while in (15) all quantities are at the same polarization; in (13) all quantities are measured or evaluated at the same frequency and polarization.

Equations (12)–(15) can be written in a form that makes explicit the unknown parameters of the drop size distribution and includes both dual-frequency and dual-polarization cases; specifically, (12) and (15) can be expressed as

$$g_1(r; D_0, \mu) = h_1(r, r_n) - 2\int_r^{r_n} N_t(s) f_1(s; D_0, \mu)\, ds, \tag{16}$$

while (13) becomes

$$g_2(r; N_t) = h_2(r, r_n; D_0, \mu) - 2\int_r^{r_n} N_t(s) f_2(s; D_0, \mu)\, ds, \tag{17}$$

with

$$\begin{aligned} g_1 &= \delta I_b(r) \\ h_1 &= \delta[\tilde{Z}_m(r) + A_r(r_n)] + \delta[A_c(r) + A_v(r)] \\ f_1 &= \delta I_e(r) \\ g_2 &= 10 \log N_t(r) \\ h_2 &= \tilde{Z}_m(r) + A_r(r_n) - I_b(r) + [A_c(r) + A_v(r)] \\ f_2 &= I_e(r), \end{aligned} \tag{18}$$

where δ is a difference operator, defined in the case of dual-polarization radar by $\delta X \equiv \delta_p X \equiv X_{\mathrm{hh}} - X_{\mathrm{vv}}$ and in the case of a dual-frequency radar by $\delta X \equiv \delta_f X \equiv X(f_1) - X(f_2)$. Note that in the case of the polarization radar, $\delta(A_c + A_v) = \delta_p(A_c + A_v) = 0$. Using the definition of I_b given by (9), the usual differential reflectivity (dB) with respect to polarization is $\delta I_b = Z_{\mathrm{dr}}$, while the dual-frequency ratio (dB) is $\delta I_b = \mathrm{DFR}$.

The constraints in the above equations are assumed to be the precipitation path attenuations at the two frequencies or two polarizations. If the constraint is total path attenuation from precipitation, cloud, and water vapor, then h_1, h_2 should be changed to

$$\begin{aligned} h_1 &= \delta\{\tilde{Z}_m + A(r_n) - [A_c(r, r_n) + A_v(r, r_n)]\}, \\ h_2 &= \tilde{Z}_m + A(r_n) - I_b - [A_c(r, r_n) + A_v(r, r_n)], \end{aligned} \tag{19}$$

where, as before,

$$A(r_n) = A_r(r_n) + A_c(r_n) + A_v(r_n). \tag{20}$$

The expressions for h_1 and h_2 in (18) and (19) are identical. However, if an independent estimate is made of the precipitation attenuation only, $A_r(r_n)$, then contributions from cloud water and water vapor to range r must be added, as in (18). If an independent estimate is made of total attenuation, then contributions from cloud water and water vapor over the range interval (r, r_n) must be subtracted, as in (19). For example, in polarimetric applications, the differential phase is well correlated with the differential attenuation from precipitation, but will be unaffected by cloud or water vapor attenuation. In contrast, for dual-wavelength airborne or spaceborne applications, if the surface reference is taken in a rain- and cloud-free environment with low water vapor, the decrease in the surface return in the presence of precipitation can be associated with the total path attenuation.

If the path attenuation is independently measured, then it can be seen from (16) and (17) that the range profiles of D_0 and N_t can be obtained by starting at the far range r_n, continuing inward toward the radar. At $r = r_n$, the integrals appearing in (16) and (17) are zero, so that D_0 can be found by numerically solving the equation $g_1(D_0, \mu) = h_1$; once D_0 is determined, it is substituted into (17) to give N_t. Proceeding to the $(n - 1)$th gate, the values of D_0 and N_t from the nth gate are substituted into the integrals in (16) and (17); because the right-hand side of (16) is determined, D_0 can be solved numerically. Substituting this into (17) gives h_2 and N_t. The recursion continues in this way until the full path is traversed.

In solving the equations numerically, the discrete forms of (16) and (17) take the form of nonlinear algebraic equations for D_0 and N_t that can be solved by Broyden's method (Press et al. 1992). For example, at the final gate, both (16) and (17) are functions of $D_0(r_n)$ and $N_t(r_n)$ if the contributions from the last gate are included. However, if the attenuation per range gate is small, the approximate and general procedures yield nearly identical results. It should also be pointed out that in some cases, such as the dual-wavelength radar returns in rain or mixed-phase hydrometeors, there can be more than one value of D_0 that satisfies (16). Procedures exist to reduce the ambiguities but not eliminate them entirely (Liao and Meneghini 2005). Moreover, because there are only two equations, the "shape" parameter μ must either be fixed or expressed as a function of the other DSD parameters (Zhang et al. 2001; Seifert 2005).

The forward integral equations take the same form as (16) and (17):

$$g_1(r; D_0, \mu) = H_1(r) + 2\int_0^r N_t(s) f_1(s; D_0, \mu)\, ds, \tag{21}$$

$$g_2(r; N_t) = H_2(r; D_0, \mu) + 2\int_0^r N_t(s) f_2(s; D_0, \mu)\, ds, \tag{22}$$

where g_1, g_2, f_1, f_2 are given by (18) and

$$\begin{aligned} H_1 &= \delta[\tilde{Z}_m(r) + A_c(r) + A_v(r)], \\ H_2 &= \tilde{Z}_m(r) - I_b(r) + A_c(r) + A_v(r). \end{aligned} \tag{23}$$

The only difference between the forward and backward equations arises from the estimates of path attenuation and differential path attenuation. Explicitly, we can write the estimates of attenuation and differential attenuation in the interval $[0, r]$ for the forward (left-hand side) and backward (right-hand side) integral equations:

$$\int_0^r N_t(s)f_1(s; D_0, \mu)\, ds \leftrightarrow \delta A(r_n) - \int_r^{r_n} N_t(s)f_1(s; D_0, \mu)\, ds,$$

$$\int_0^r N_t(s)f_2(s; D_0, \mu)\, ds \leftrightarrow A(r_n) - \int_r^{r_n} N_t(s)f_2(s; D_0, \mu)\, ds.$$

Equations (21)–(23) are independent of a path attenuation estimate and are naturally solved in the forward direction from the radar outward, although, as Mardiana et al. (2004) and Iguchi (2005) have pointed out, this is not required. The basic forms of the forward and backward equations are the same except that the path attenuation to range r in the forward equations is expressed in terms of the size distribution parameters obtained from prior gates between the range of interest and the radar. Despite the similarities between (16)–(18) and (21)–(23), the two formulations show significant differences in performance, as will be shown in section 4.

3. Equations based on the *kZ* parameterization

Testud et al. (2000) and Bringi et al. (2001) recognized that techniques developed for single attenuating-wavelength radars can be applied to polarimetric radar data at attenuating wavelengths. These methods are a subset of a larger class of polarimetric attenuation correction methods reviewed by Bringi and Chandrasekar (2001). Extensions of the basic approach have been proposed as well (e.g., Lim and Chandrasekar 2006). Although most formulations begin with the final value solution of Marzoug and Amayenc (1991, 1994), an equivalent form follows directly from the "α adjustment" solution (Meneghini et al. 1983; Iguchi and Meneghini 1994), where, taking 10 log of (19) of Iguchi and Meneghini (1994), gives ($r \le r_n$)

$$\tilde{Z}(r) = \tilde{Z}_m(r) - \beta^{-1} 10 \log Q, \tag{24}$$

where

$$k = \alpha Z^{\beta}, \tag{25}$$

$$S(r) = \int_0^r \alpha(s) Z_m^{\beta}(s)\, ds, \tag{26}$$

$$Q = 1 + (10^{-0.1\beta A(r_n)} - 1)[S(r)/S(r_n)]. \tag{27}$$

In the above equations, the parameter β must be taken as constant in range, whereas α is allowed to vary in range. An example of this is a path along which distinct regions of frozen, mixed-phase, and liquid precipitation are present. However, if α can be considered constant with range, then (24) is independent of this parameter.

For constant α along the path, (24) can also be obtained by taking the expression for k from the final value solution [(24) of Testud et al. (2000)], integrating it from 0 to r and using the definition of Z_m:

$$\tilde{Z}(r) = \tilde{Z}_m(r) + 2\int_0^r k(s)\, ds. \tag{28}$$

For polarimetric applications, the two-way path attenuation $A(r_n)$ can be estimated by the differential phase shift over the path $\Delta\Phi_{\rm dp}$ (°) by using a relationship between k and $\kappa_{\rm dp}$ (° km^{-1}) (Testud et al. 2000; Matrosov et al. 2002; Anagnostou et al. 2004). In the case of a linear k–$\kappa_{\rm dp}$ relationship:

$$k_{pp} = \gamma_{pp}\kappa_{\rm dp}, \tag{29}$$

then

$$A_{pp}(r_n) = 2\int_0^{r_n} k_{pp}(s)\, ds = 2\gamma_{pp}\int_0^{r_n} \kappa_{dp}(s)\, ds = \gamma_{pp}\Delta\Phi_{\rm dp}(0, r_n). \tag{30}$$

For the results to apply to dual-frequency as well as dual-polarization data, we use the two-way path attenuation $A(r_n)$ instead of $\Delta\Phi_{\rm dp}$. In deriving equations similar to those obtained for the integral equation approach, it is convenient to write (27) in the form

$$Q = 10^{-0.1\beta A(r_n)}\{10^{0.1\beta A(r_n)} + [1 - 10^{0.1\beta A(r_n)}][S(r)/S(r_n)]\}, \tag{31}$$

so that (24) becomes

$$\tilde{Z}(r) = \tilde{Z}_m(r) + A(r_n) - \beta^{-1} 10 \log \tilde{Q}, \tag{32}$$

where

$$\tilde{Q} = 10^{0.1\beta A(r_n)} + [1 - 10^{0.1\beta A(r_n)}][S(r)/S(r_n)]. \tag{33}$$

Using (32), equations analogous to (12) and (13) can be obtained by expressing $\tilde{Z}_{m,pp}(r, f)$ and $\tilde{Z}_{m,\rm hh}(r, f) - \tilde{Z}_{m,\rm vv}(r, f)$ in terms of D_0 and N_t:

$$I_{b,\rm hh}(r) - I_{b,\rm vv}(r) = [\tilde{Z}_{m,\rm hh}(r) - \tilde{Z}_{m,\rm vv}(r)] + [A_{\rm hh}(r_n) - A_{\rm vv}(r_n)] - 10 \log[\tilde{Q}_{\rm hh}{}^{1/\beta_{\rm hh}}/\tilde{Q}_{\rm vv}{}^{1/\beta_{\rm vv}}], \tag{34}$$

$$\tilde{N}_t(r) = \tilde{Z}_m(r) - I_b(r) + A(r_n) - \beta^{-1}10\log\tilde{Q} + A_c(r) + A_v(r), \quad (35)$$

where $\tilde{N}_t \equiv 10\log N_t$.

As before, we have suppressed the subscripts in (35) because all relevant quantities are evaluated at the same polarization. Other quantities in (34) and (35) are defined above, but without subscripts. Explicitly,

$$\tilde{Q}_{pp} = 10^{0.1\beta_{pp}A_{pp}(r_n)} + [1 - 10^{0.1\beta_{pp}A_{pp}(r_n)}] \times [S_{pp}(r)/S_{pp}(r_n)], \quad (36)$$

$$S_{pp}(r) = \int_0^r \alpha_{pp}(s)Z_{m,pp}^{\beta_{pp}}(s)\,ds. \quad (37)$$

For the kZ backward formulation, equations that include dual-frequency and dual-polarization cases can be written in a form similar to (16) and (17):

$$g_1(r; D_0, \mu) = h_1(r, r_n) - 10\delta(\log\tilde{Q}^{1/\beta}), \quad (38)$$

$$g_2(r; N_t) = h_2(r, r_n; D_0, \mu) - 10\log\tilde{Q}^{1/\beta}, \quad (39)$$

where g_1, g_2, h_1, and h_2 are given by (18). In the dual-frequency radar case, the last term in (38) becomes

$$\delta(\log\tilde{Q}^{1/\beta}) \equiv \delta_f(\log\tilde{Q}^{1/\beta}) = \beta^{-1}(f_1)\log\tilde{Q}(f_1) - \beta^{-1}(f_2)\log\tilde{Q}(f_2). \quad (40)$$

Comparison between (16)–(17) and (38)–(39) show that the only differences between the two sets of equations are the terms

$$2\int_r^{r_n} N_t(s)\delta I_e(s)\,ds \leftrightarrow 10\delta(\log\tilde{Q}^{1/\beta}), \quad (41)$$

$$2\int_r^{r_n} N_t(s)I_e(s)\,ds \leftrightarrow \beta^{-1}10\log\tilde{Q}.$$

The right- and left-hand sides of (41) represent the different ways in which the equations account for the attenuation and differential attenuation in the range interval from r to r_n. In the (backward) integral equation approach, the interval attenuations are expressed as functions of the DSD parameters obtained from previous steps in the recursion. In the kZ formulation, the attenuations are estimated by means of the kZ parameterization using path attenuation and measured radar reflectivity factors in the range from r to r_n. In both of these backward-going solutions, the contributions are subtracted from the total path attenuation to obtain an estimate of attenuation to range r.

It is worth pointing out that forward equations based on the kZ parameterization can be obtained directly from the Hitschfeld–Bordan equation, and can be written in a form similar to that of (38) and (39). However, the estimates for N_t and D_0 based on these equations are highly sensitive to attenuation and errors in the various parameters, so that these equations will not be considered here.

4. Comparisons of formulations for an X-band polarimetric radar

To illustrate some aspects of the solutions to the equations based on the integral and kZ formulations, we construct a simulation for an X-band polarimetric radar using disdrometer-measured raindrop size distributions as the input data. We assume a 50-km path consisting of 250 gates with 0.2-km range resolution. In the general case, a sequence of 250 one-minute-averaged DSDs provides the particle number concentration and median mass diameter at each range gate. However, to better understand the behavior of the equations, the DSD parameters, and therefore the rain rates, are assumed to be constant in range. Assuming the Beard and Chuang (1987) shape–size relationship and a fixed μ value along the path, the simulated range profiles of the measured radar reflectivity factors at the two polarizations are calculated, that is, $[Z_{m,\mathrm{hh}}(r_j), Z_{m,\mathrm{vv}}(r_j)]$; $j = 1, \ldots, 250$. To further simplify the discussion, we assume infinite signal-to-noise ratios without fluctuations in the Z fields from finite sampling. Moreover, the shape–size relationship is assumed to be exact and without raindrop canting.

For the backward recursion, the integral and kZ approaches reduce to the same set of equations at the nth gate. In particular, (12) and (34) at $r = r_n$ reduce to

$$I_{b,\mathrm{hh}}(r_n) - I_{b,\mathrm{vv}}(r_n) = [\tilde{Z}_{m,\mathrm{hh}}(r_n) - \tilde{Z}_{m,\mathrm{vv}}(r_n)] + [A_{\mathrm{hh}}(r_n) - A_{\mathrm{vv}}(r_n)]. \quad (42)$$

Also, if cloud and water vapor attenuations are neglected, (13) and (35) become

$$\tilde{N}_t(r_n) = \tilde{Z}_m(r_n) - I_b(r_n) + A(r_n). \quad (43)$$

The sensitivity to several types of errors can be inferred from these equations. For example, if the differential measured reflectivity and differential path attenuation are unbiased, then $Z_{\mathrm{dr}} = I_{b,\mathrm{hh}} - I_{b,\mathrm{vv}}$ is unbiased. However, if $\mu > \mu_T$, where the T subscript denotes the true or input value, then it can be seen from the top left-hand plot in Fig. 1 that $D_0 > D_{0,T}$. Also, because I_b, I_e, δI_e are derived from the estimated median mass diameter, these quantities will also be positively biased as can be seen from an inspection of the I_b, I_e, and δI_e plots

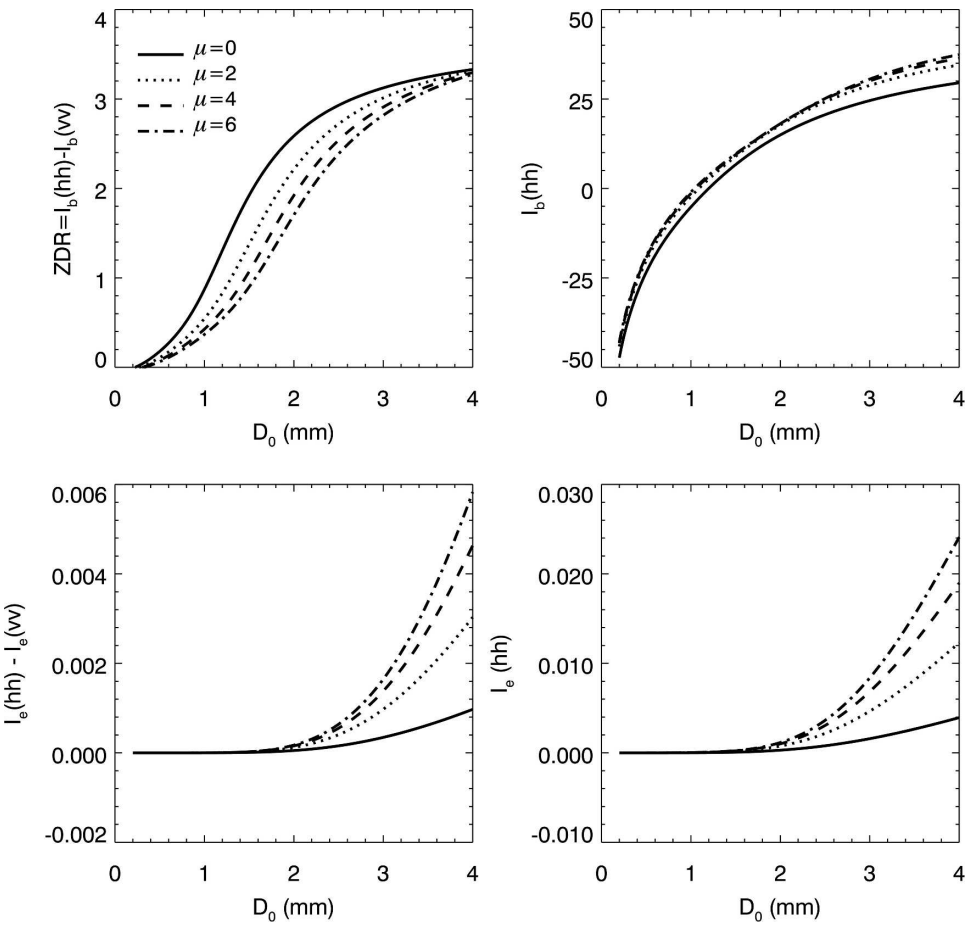

FIG. 1. Parameters of the polarization radar at 10 GHz vs median mass diameter D_0 for several values of the shape parameter μ.

in Fig. 1. From (43) it follows that an overestimate in I_b, in the absence of other errors, yields an underestimate in N_t. The opposite behavior occurs if $\mu < \mu_T$. These relationships can be summarized by the following inequalities:

$$\mu > \mu_T \Rightarrow D_0 > D_{0,T}, N_t < N_{t,T},$$
$$\mu < \mu_T \Rightarrow D_0 < D_{0,T}, N_t > N_{t,T}.$$

If the right-hand side of (42) and μ are unbiased, then D_0, I_b are unbiased. In this case the bias in $\tilde{N}_t$ is determined solely by the bias in the quantity $\tilde{Z}_m + A(r_n)$.

Although the two formulations yield the same results at the final gate, the estimates generally exhibit significant differences with range. Figures 2 and 3 show the range dependence of rain rate (Fig. 2) and D_0 (Fig. 3) estimates for $\mu = (0,2,6)$, where $\mu_T = 2$. In all cases, the rain rate is derived from the estimated (N_t, D_0) and assumed μ value. Input values of rain rate, path attenuation, and differential path attenuation are R_T = 12.5 mm h^{-1}; $A_{\mathrm{hh},T}(r_n)$ = 33 dB; $A_{\mathrm{hh},T}(r_n) - A_{\mathrm{vv},T}(r_n)$ = 5.6 dB. In each figure, the results from the kZ parameterization [(34) and (35)] are shown in the upper panel, and results from the integral equations [(12) and (13)] are shown in the lower panel. Unless stated otherwise, all results are obtained from a backward recursion. To understand why the results from the kZ parameterization are range independent, note that (34) and (35) are identical to (42) and (43) except for the attenuation correction terms involving $\tilde{Q}$. But, these terms are determined solely by the path attenuations and the measured radar reflectivity factors, and are independent of the DSD parameters derived at other range gates. As will be seen in subsequent examples, only errors in the path attenuation yield range dependencies in the kZ attenuation correction method.

One other feature of Fig. 2 and subsequent results is that even in the absence of errors, the estimated quantity (in this case rain rate) differs from the input value. There are two reasons for this. The first is that D_0 is estimated by means of a third-order polynomial in Z_{dr}.

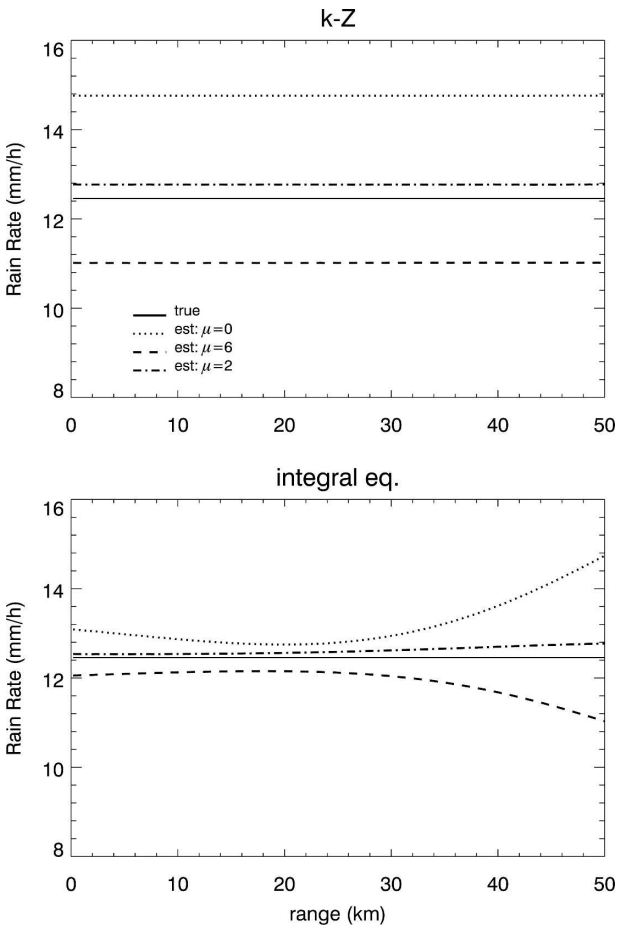

FIG. 2. Rain-rate estimates from the (top) kZ and (bottom) integral equation formulations for three values of the assumed shape parameter with input value, $\mu_T = 2$.

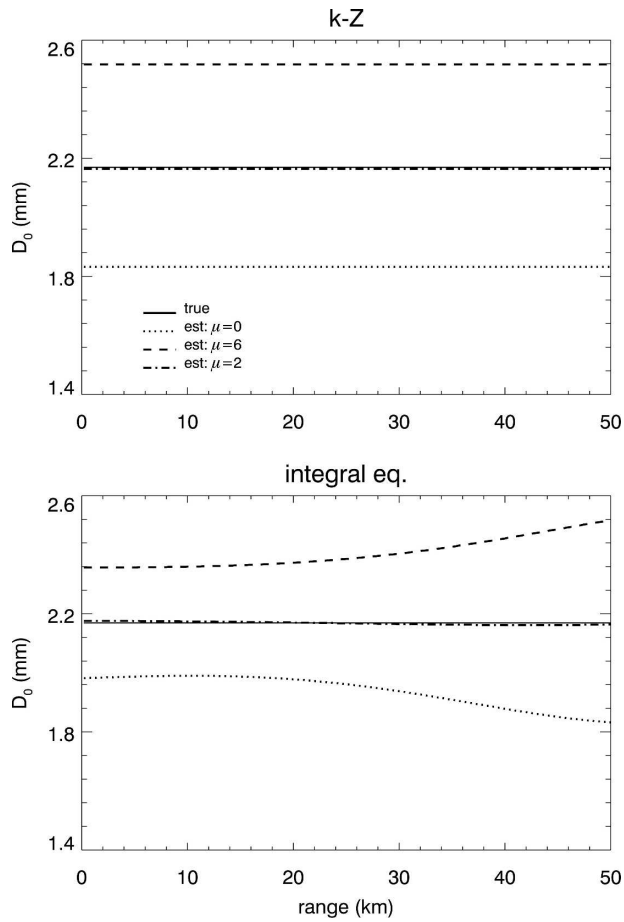

FIG. 3. Estimates of median mass diameter from the (top) kZ and (bottom) integral equation formulations for three values of the assumed shape parameter, with input value $\mu_T = 2$.

Although the fit is fairly accurate, small errors in D_0 can translate into larger errors in rain rate. A second source of error arises in estimating I_b, I_e, and δI_e from D_0 via lookup tables and a linear interpolation. (For the kZ parameterization only the $I_b - D_0$ relationship is needed.) Improvements in accuracy can be made by replacing the $D_0 - Z_{\mathrm{dr}}$ fit with a lookup table and using more finely sampled lookup tables for estimating I_b, I_e, and δI_e.

For the integral equations, the D_0 estimated from (12) is used to determine both I_b and I_e that are then used in (13). Moreover, the N_t obtained in (13), along with the D_0 from previous steps, determines the differential attenuation term given by the last term in (12). This strong linkage between the equations usually produces a negative feedback where the biases are reduced in magnitude when progressing toward ranges closer to the radar. To see this in detail in the present case, consider the $\mu = 6$ example. As noted above, because $\mu > \mu_T$, D_0 is overestimated and N_t is underestimated at the nth gate. At the $(n - 1)$th gate, the negatively biased N_t value, along with the positively biased δI_e term, is used to determine the differential attenuation term in (12). Initially, at the far ranges, this produces a somewhat larger value than the true value and therefore a smaller value for the right-hand side of (12). This yields, in turn, a slight decrease in D_0 from its value at the nth gate. From Fig. 1, a decrease in D_0 produces a decrease in I_b and, in accordance with (13), a reduction in the negative bias of N_t. For the curves in the bottom panel of Fig. 2, an inspection of the numerical results shows that feedback becomes slightly positive for ranges less than 18.4 km for $\mu = 6$ and less than 19.2 km for $\mu = 0$.

Negative feedback in the integral equation solutions also occurs for offset errors in Z. For the example shown in Figs. 4–6, the bias in the differential reflectivity factor is assumed to zero, but with offsets in $\tilde{Z}_{\mathrm{hh}}$, $\tilde{Z}_{\mathrm{vv}}$ of +2, −2, or 0. The input data for these examples are $R_T = 10.5$ mm h^{-1}; $A_{\mathrm{hh},T}(r_n) = 17.5$ dB; $A_{\mathrm{hh},T}(r_n) -$

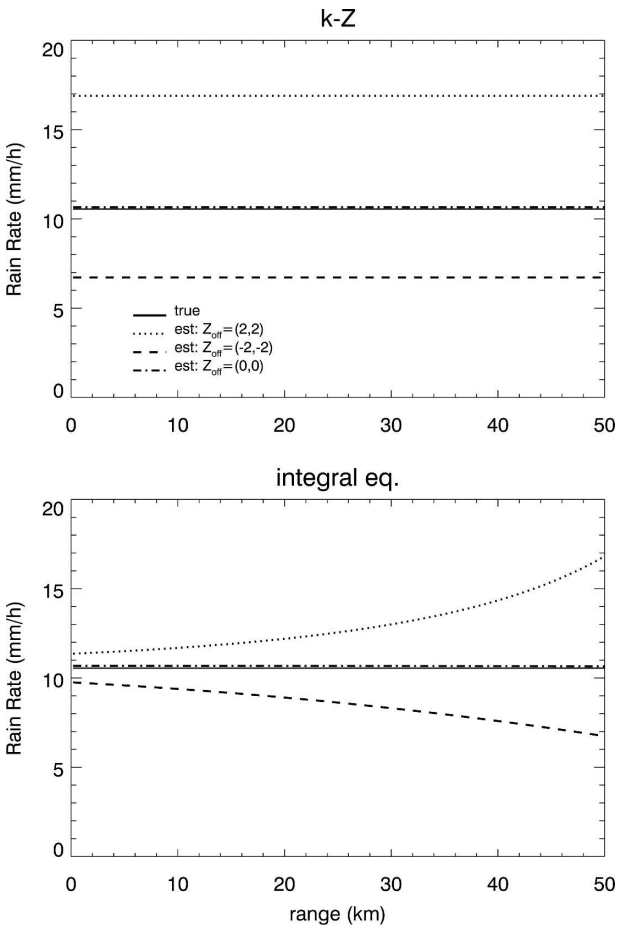

FIG. 4. Rain-rate estimates from the (top) kZ and (bottom) integral equation formulations for offset errors in the radar reflectivity factors.

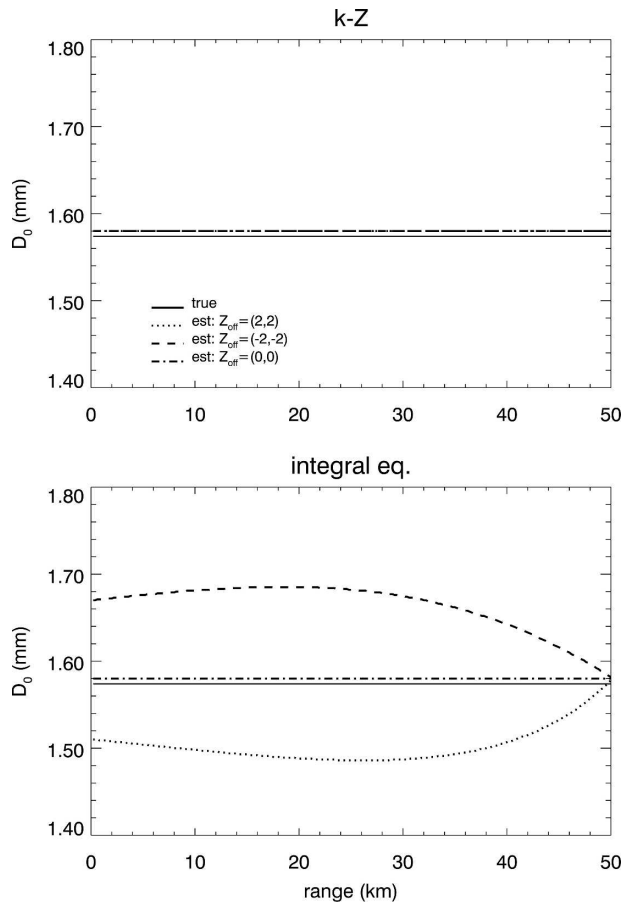

FIG. 5. Estimates of median mass diameter from the (top) kZ and (bottom) integral equation formulations for offset errors in the radar reflectivity factors.

$A_{\mathrm{vv},T}(r_n) = 2.2$ dB. The range dependences of R, D_0, and $\tilde{N}_t$ are shown in Figs. 4–6, respectively. At the final gate, and for both solutions, D_0 is unbiased while the biases in N_t are determined by the biases in the $\tilde{Z}_{\mathrm{hh}}$, $\tilde{Z}_{\mathrm{vv}}$ terms. In the kZ approach, D_0 remains unbiased over the full range and the biases in R and N_t remain constant with range. For the integral equation solution, in the negatively biased Z case, the underestimate in N_t produces an underestimate in the differential attenuation term $\int_r^{r_n} N_t \delta I_e \, ds$ in (12), which produces an overestimate in D_0 as shown in Fig. 5. This overestimate in D_0 produces an overestimate in I_b, which, according to (13), reduces the bias in N_t. For positive $\tilde{Z}_{\mathrm{hh}}$, $\tilde{Z}_{\mathrm{vv}}$ biases, the effects are reversed; in particular, a positive bias in $\tilde{Z}_{\mathrm{hh}}$, $\tilde{Z}_{\mathrm{vv}}$ produces an identical bias in $\tilde{N}_t$. This leads to underestimates in D_0 and I_b that reduce the positive bias in $\tilde{N}_t$.

An inspection of (12) and (13) shows that a bias in $\tilde{Z}_{\mathrm{hh}}(r)$ has the same effect on the solutions as does an identical bias in $A_{\mathrm{hh}}(r_n)$. Likewise, a bias in $\tilde{Z}_{\mathrm{hh}}(r) - \tilde{Z}_{\mathrm{vv}}(r)$ is equivalent to a bias in $A_{\mathrm{hh}}(r_n) - A_{\mathrm{vv}}(r_n)$. This equivalence does not hold for the kZ formulation. As seen in the previous example, offsets in $\tilde{Z}_{\mathrm{hh}}(r)$ produce kZ-derived solutions that are constant in range. Offsets in $A_{\mathrm{hh}}(r_n)$, however, produce range-dependent solutions. Moreover, unlike the integral equation method, the kZ-based results converge to the input values as the radar range goes to zero. This behavior is shown in Fig. 7, where the kZ solutions are shown for R, D_0, and N_t for offsets in $A_{\mathrm{hh}}(r_n)$, $A_{\mathrm{vv}}(r_n)$ of 2, −2, and 0 dB. The integral equation results are displayed in the lower panels of Figs. 4–6 because they are identical to the Z-offset case. To understand the behavior of the kZ solutions in this case, note that the $\log(\tilde{Q})$ and $\delta \log(\tilde{Q})$ terms in (34) and (35) are functions of the path attenuations that play the same role as the corresponding terms in the integral equations. In particular, these terms function as negative feedback, reducing the magnitude of the biases as the radar range decreases. Unlike the integral

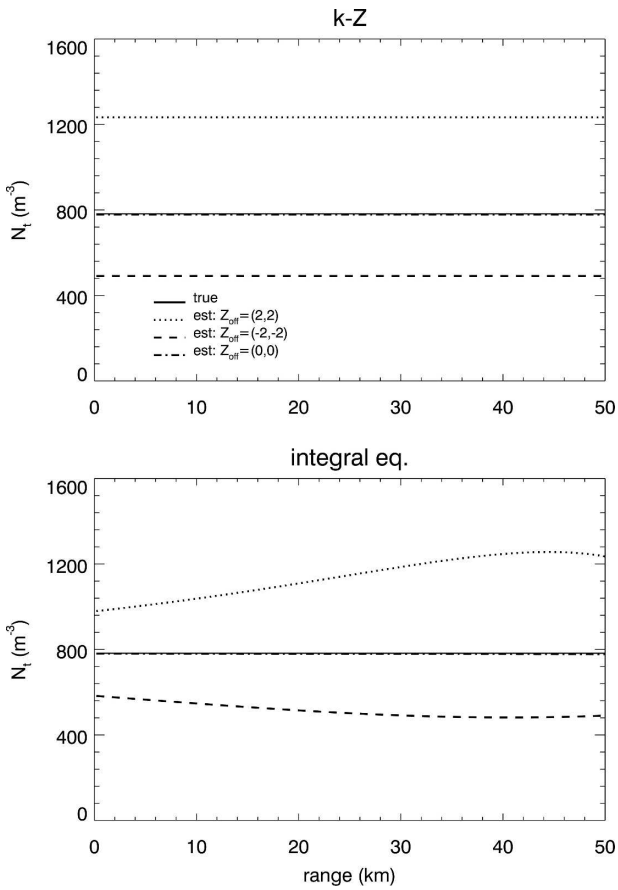

FIG. 6. Estimates of particle number concentration from the (top) kZ and (bottom) integral equation formulations for offset errors in the radar reflectivity factors.

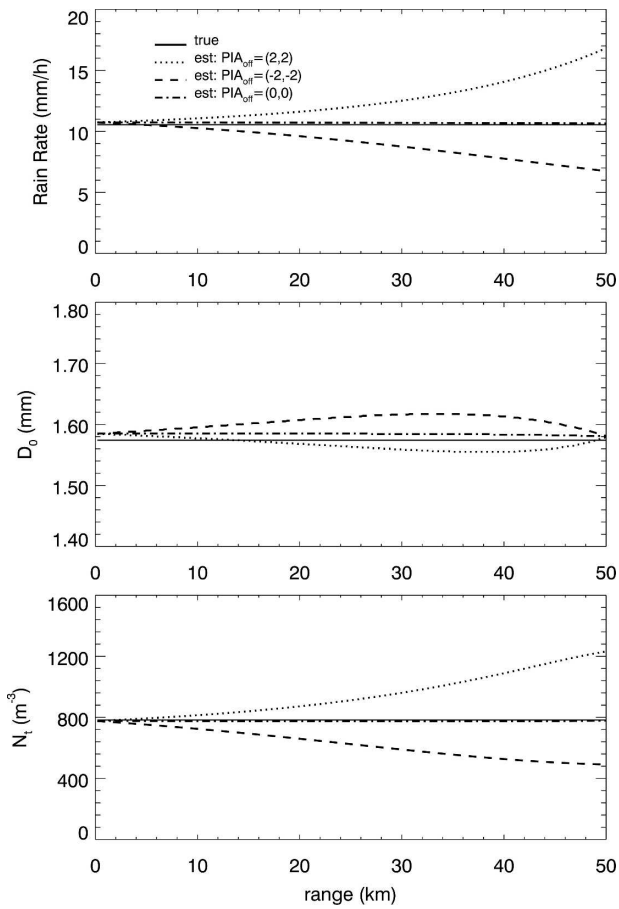

FIG. 7. Estimates of (top) rain rate, (middle) median mass diameter, and (bottom) number concentration using the kZ formulation for errors in the path attenuations.

equations, however, the kZ formulation yields exact solutions in the absence of other errors. This follows from (36) by noting that as $r \to 0$, $\tilde{Q}_{pp} = 10^{0.1\beta_{pp}} A_{pp}(r_n)$, so that the last term in (35) exactly cancels the quantity $A(r_n)$. In a similar way, the last term in (34) cancels the quantity $A_{\mathrm{hh}}(r_n) - A_{\mathrm{vv}}(r_n)$ so that the equations reduce to the dual-polarization equations in the absence of attenuation.

In the examples given, moderate rain rates were used. Similar characteristics of the solutions are observed at lighter rain rates and path attenuations. However, because of the nonlinear nature of the equations, the qualitative behavior of the solution can change abruptly as the rain rate and path attenuation increase. For the rain-rate estimates shown in Fig. 8, values of $\mu = [0, 2, 6]$ are assumed, where $\mu_T = 2$. In this case, the input rain rate, path attenuation, and differential path attenuation are given by $R_T = 21.5$ mm h^{-1}; $A_{\mathrm{hh},T}(r_n) = 65$ dB; $A_{\mathrm{hh},T}(r_n) - A_{\mathrm{vv},T}(r_n) = 12$ dB. Recall that the same assumptions regarding μ are used for the results in the lighter rain-rate case shown in Fig. 2. Except for evidence of numerical instabilities in the kZ formulation at the far ranges (Fig. 8, top panel), the results are qualitatively similar to those in Fig. 2 (top panel). In contrast, the integral equation solution, shown in the bottom panel of Fig. 8, exhibits a slight oscillatory behavior so that in moving toward the radar from the far range the error first decreases, attaining a minimum at about 36 km, and then begins gradually to increase, attaining a maximum at 19.4 km for $\mu = 0$ and a maximum at 8.6 km for $\mu = 6$. At closer ranges, the error once more decreases.

For the results in Fig. 9 the same raindrop size distribution is used, but the behavior of the solutions are shown for errors in the path attenuation where A_{hh} and A_{vv} are either both positively or negatively biased by 2 dB. The kZ solution is qualitatively similar to that shown in Fig. 7 (top panel) except for numerical instabilities at the far ranges. However, unlike the result shown in the bottom panel of Fig. 4, the integral equation solution for rain rate (as well as for D_0 and N_t)

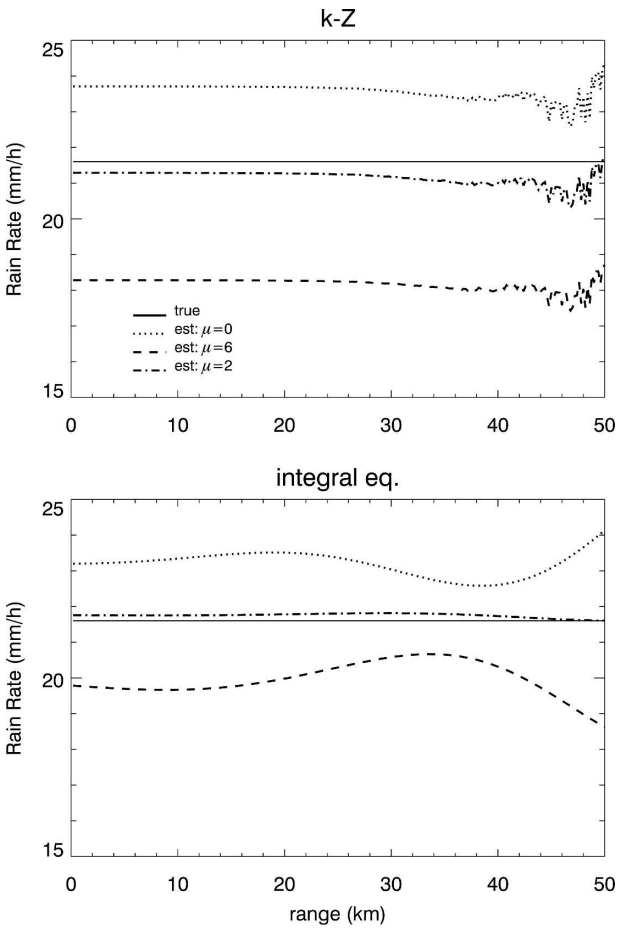

FIG. 8. Rain-rate estimates from the (top) kZ and (bottom) integral equation formulations for three values of the assumed shape parameter with input value, $\mu_T = 2$.

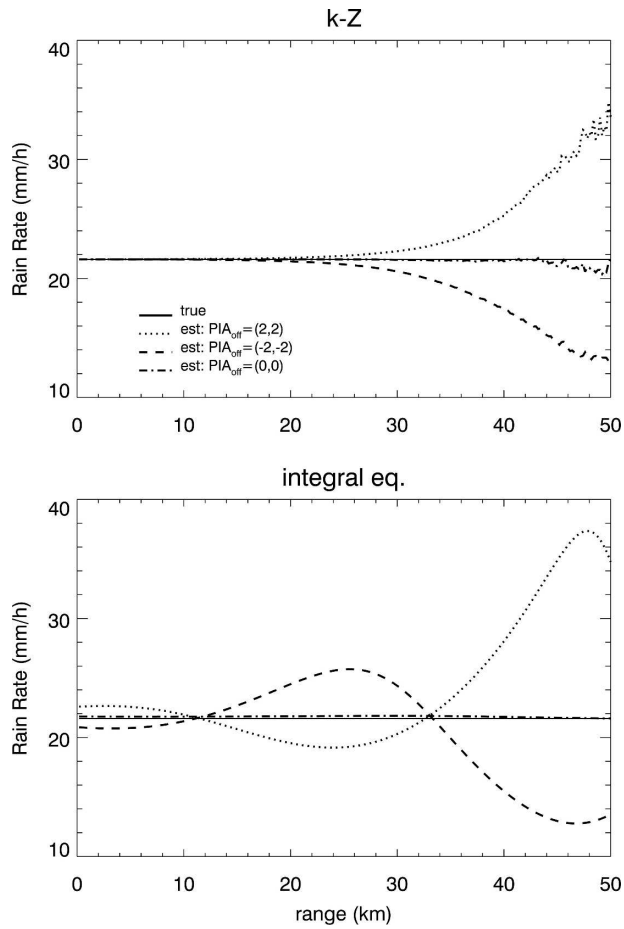

FIG. 9. Rain-rate estimates from the (top) kZ and (bottom) integral equation formulations for errors in the path attenuations.

exhibits a damped oscillatory behavior about the true value. As the rain rate and path attenuation are further increased, the integral equations continue to yield damped oscillatory behavior, but with an increase in amplitude and frequency. For the kZ solution, numerical instabilities restrict the solution to ranges near the radar. The reason for the instability can be seen from (36) where, for large values of attenuation, $S_{pp}(r)$ rapidly approaches $S_{pp}(r_n)$ as r increases, so that $\tilde{Q}$ is computed from the difference of large quantities that are nearly equal in magnitude. An improvement in stability can be obtained by writing (36) in the form

$$\tilde{Q}_{pp} = 10^{0.1\beta_{pp}A_{pp}(r_n)}\{[S_{pp}(r_n) - S_{pp}(r)]/S_{pp}(r_n)\} + S_{pp}(r)/S_{pp}(r_n).$$

However, this form is subject to an instability similar to that which occurs in the Hitschfeld–Bordan equation; that is, for large attenuation, the term $S_{pp}(r_n) - S_{pp}(r)$ rapidly approaches zero as $r \to r_n$, so that $\tilde{Q}$ is computed from the multiplication of a very large and a very small number.

To investigate the oscillatory nature of the integral equation solutions for large path attenuation, we use phase-state diagrams (Fig. 10) in which the (D_0, N_t) values as a function of radar range are represented by a trajectory in (D_0, N_t) space. The input values of (D_0, N_t), assumed constant in range, is represented by an "X" and the range-dependent solution to the integral equation are represented by a curve that begins at 50 km (indicated by the box around the point), which spirals in a counterclockwise direction toward the input value. For the upper panels in Fig. 10, errors in Z_{hh}, Z_{vv} of 2 dB are assumed; for the lower panels errors in Z_{hh}, Z_{vv} of -2 dB are assumed. In moving from left to right, the input D_0 increases from 2.1 (left) to 2.4 (middle) to 2.7 (right) mm. For all cases, the assumed value of N_t is taken to be 600 m^{-3}. The results show that as D_0 and path attenuation increase, the amplitude and frequency

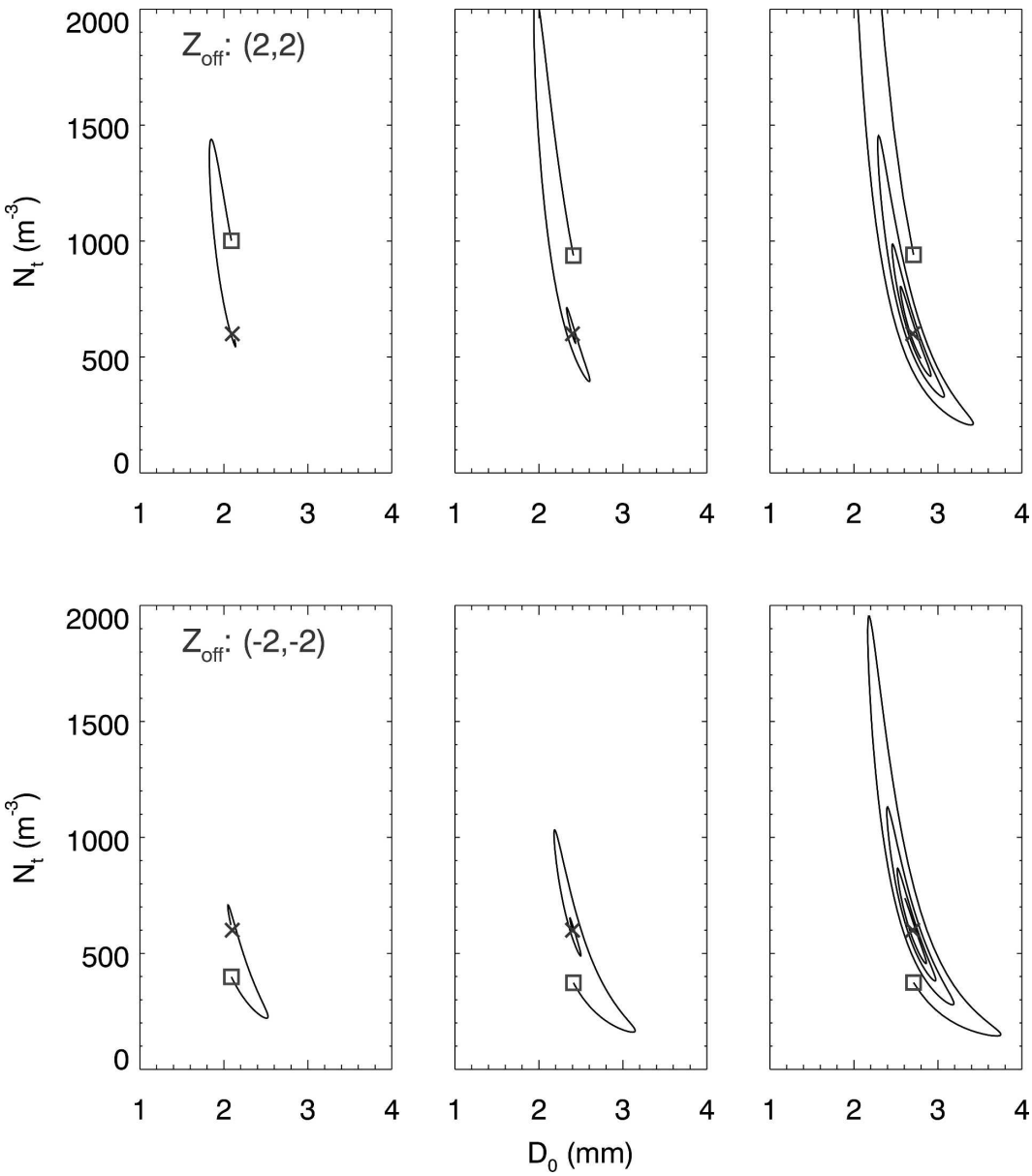

FIG. 10. Solutions of integral equation for (D_0, N_t). Solution at 50 km from the radar is enclosed by box; counterclockwise trajectory from this point represents decreasing radar range. Input (D_0, N_t) value is represented by "X." (top) Solutions for +2 dB offset in Z_{hh}, Z_{vv}; (bottom) solutions for −2 dB offset in Z_{hh}, Z_{vv}. Input values of D_0 from (left) 2.1, (middle) 2.4, and (right) 2.7 mm.

of the oscillations increase. On the other hand, as the radar range decreases, the amplitude is damped and the solution spirals in toward the input values. As pointed out earlier, at the farthest range (50 km), the value of D_0 is unbiased while the bias in N_t is determined by the bias in the radar reflectivity factors. Although our focus is on the behavior of the dual-polarization equations, it is worth noting that for the dual-wavelength integral equations, oscillatory solutions do not occur and that the error decreases uniformly with decreasing range. This appears to result from the differences in sign between the δI_b, δI_e for the two situations; in particular, for the dual-polarization data, these quantities are of the same sign (as seen by the data in upper and lower left-hand panels of Fig. 1), whereas in the dual-wavelength tables for 13.6 and 35.5 GHz, δI_b, δI_e are of opposite sign for D_0 greater than about 1 mm.

Although the backward formulations are generally preferable because of their more robust behavior, some features of the forward integral equations are worth

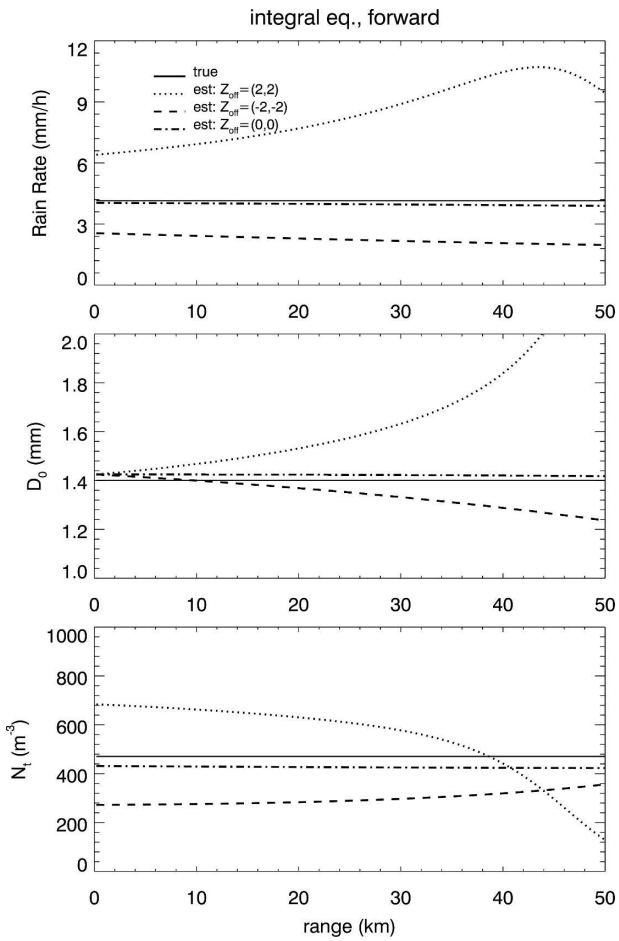

FIG. 11. Estimates of (top) rain rate, (middle) median mass diameter, and (bottom) number concentration using the forward integral equation formulation for offset errors in the radar reflectivity factors.

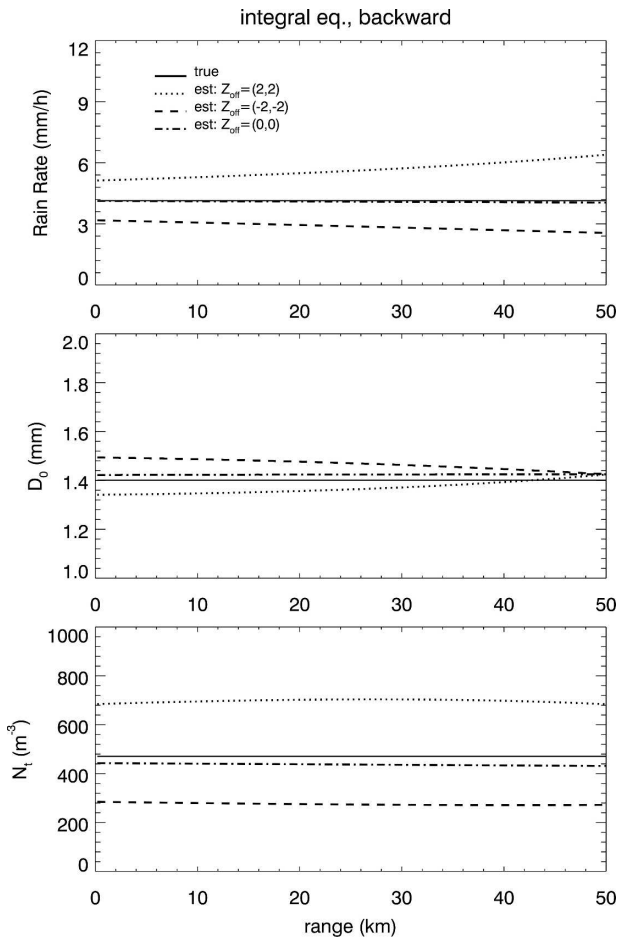

FIG. 12. Estimates of (top) rain rate, (middle) median mass diameter, and (bottom) number concentration using the backward integral equation formulation for offset errors in the radar reflectivity factors.

noting. As mentioned in section 2, for the backward recursion, the interval attenuation $[r, r_n]$ is subtracted from the total attenuation, while in the forward case it is simply the interval attenuation $[0, r]$ that is used in the equations. In the backward recursion, the bias errors are usually reduced by negative feedback; in the forward recursion, however, the bias errors from this term are usually amplified by positive feedback. This difference between the formulations leads to behavior in which errors in the forward solution grow rapidly with increasing attenuation. On the other hand, because the method does not require an estimate of path attenuation, it can have better accuracies than the backward solutions for either light rain rates or when the independent estimate of path attenuation is inaccurate. In Figs. 11–12 estimates of R, D_0, and N_t are shown for the forward and backward integral equations, respectively, for the case of calibration errors in Z of 0 and ± 2 dB. Even in this relatively light rain-rate case [$R_T = 4.1$ mm/h; $A_{\mathrm{hh},T}(r_n) = 5$ dB; $A_{\mathrm{hh},T}(r_n) - A_{\mathrm{vv},T}(r_n) = 0.6$ dB], instabilities in the forward estimates can be seen, particularly in the D_0 estimates shown in the center panel of Fig. 11. On the other hand, in the absence of errors in Z but with errors in the path attenuations, the forward estimates (given by the zero offset case in Fig. 11) would generally be more accurate than those from either of the backward recursion methods.

As noted by Iguchi (2005), the backward integral equations without path attenuation constraints (Mardiana et al. 2004) are mathematically the same as the forward integral equations given here. For light rain-rate cases, this has been verified using the present simulation. Although the solutions diverge as the rain rate increases, this can be attributed to numerical instabilities in both formulations. For the modified backward iterative procedure of Rose and Chandrasekar (2006),

we expect a similar equivalence to an appropriately modified forward procedure. However, this has not been checked.

5. Discussion and summary

Integral equations for the parameters of the particle size distribution have several useful features in that they explicitly include path attenuation constraints and provide attenuation correction in terms of the particle size distribution parameters determined in earlier steps (range gates) of the procedure. Because the dual-wavelength and dual-polarization radar data are governed by essentially the same equations, a common theoretical framework is provided by which errors in the retrievals can be assessed. This should be beneficial to the proposed Global Precipitation Measurement Mission (Iguchi et al. 2002) where quantities derived from a dual-wavelength spaceborne radar can be expected to be compared with similar quantities derived from ground-based dual-polarization radars. Making good use of these data will depend on an understanding of the inherent errors in both spaceborne and ground-based algorithms.

By using the kZ parameterization, similar sets of equations applicable to dual-wavelength and dual-polarization radars can be derived. For the polarization radar, these equations are similar in content to those derived by Testud et al. (2000) and Bringi et al. (2001), and recently analyzed by Gorgucci and Chandrasekar (2005). As illustrated in the examples of section 4, despite differences, the two formulations function in a somewhat similar manner. Advantages of the integral equation approach were noted in cases of errors in the shape parameter μ or in Z. On the other hand, the kZ formulation was seen to be more accurate than the integral equation solution in the presence of errors in path attenuation.

In a study comparing what is here called the kZ formulation with an attenuation correction obtained directly from the differential phase estimate (Matrosov et al. 2002), Gorgucci and Chandrasekar (2005) concluded that neither approach was best in all cases. A similar conclusion can be drawn for the kZ and integral equation approaches, implying that for polarimetric data at attenuating wavelengths, comparisons among the three approaches should be useful as a diagnostic tool. Comparisons of results from kZ and integral equation formulations should also be useful for dual-wavelength data.

It is worth noting that apart from the integral equation and kZ parameterization formulations, other dual-wavelength techniques have been proposed (e.g., Marzoug and Amayenc 1994; Adhikari and Nakamura 2003; Grecu and Anagnostou 2004; Iguchi 2005). In view of the close relationship between dual-wavelength and dual-polarization algorithms, some of these formulations may also be applicable to both types of data.

REFERENCES

Adhikari, N. B., and K. Nakamura, 2003: Simulation-based analysis of rainrate estimation errors in dual-wavelength precipitation radar from space. *Radio Sci.,* **38,** 1066, doi:10.1029/2002RS002775.

Anagnostou, E. N., M. N. Anagnostou, W. F. Krajewski, A. Kruger, and B. J. Miriovsky, 2004: High-resolution rainfall estimation from X-band polarimetric radar measurements. *J. Hydrometeor.,* **5,** 110–128.

Battan, L. J., 1973: *Radar Observation of the Atmosphere*. University of Chicago Press, 324 pp.

Beard, K. V., and C. Chuang, 1987: A new model for the equilibrium shape of raindrops. *J. Atmos. Sci.,* **44,** 1509–1524.

Bringi, V. N., and V. Chandrasekar, 2001: *Polarimetric Doppler Weather Radar: Principles and Applications*. Cambridge University Press, 636 pp.

——, T. D. Keenan, and V. Chandrasekar, 2001: Correcting C-band radar reflectivity and differential reflectivity data for rain attenuation: A self-consistent method with constraints. *IEEE Trans. Geosci. Remote Sens.,* **39,** 1906–1915.

Gorgucci, E., and V. Chandrasekar, 2005: Evaluation of attenuation correction methodology for dual-polarization radars: Application to X-band systems. *J. Atmos. Oceanic Technol.,* **22,** 1195–1206.

Grecu, M., and E. N. Anagnostou, 2004: A differential attenuation based algorithm for estimating precipitation from dual-wavelength spaceborne radar. *Can. J. Remote Sens.,* **30,** 697–705.

Hitschfeld, W., and J. Bordan, 1954: Errors inherent in the radar measurement of rainfall at attenuating wavelengths. *J. Meteor.,* **11,** 58–67.

Iguchi, T., 2005: A possible algorithm for the dual-frequency radar on the Global Precipitation Mission. *Proc. 32d Conf. on Radar Meteorology,* Albuquerque, NM, Amer. Meteor. Soc., CD-ROM, 5R.4.

——, and R. Meneghini, 1994: Intercomparison of single-frequency methods for retrieving a vertical rain profile from airborne or spaceborne radar data. *J. Atmos. Oceanic Technol.,* **11,** 1507–1516.

——, R. Oki, E. A. Smith, and Y. Furuhama, 2002: Global Precipitation Measurement program and the development of dual-frequency precipitation radar. *J. Commun. Res. Lab. (Japan),* **49,** 37–45.

Liao, L., and R. Meneghini, 2005: A study of air/space-borne dual-wavelength radar for estimates of rain profiles. *Adv. Atmos. Sci.,* **22,** 841–851.

Lim, S., and V. Chandrasekar, 2006: A dual-polarization rain profiling algorithm. *IEEE Trans. Geosci. Remote Sens.,* **44,** 1011–1021.

Mardiana, R., T. Iguchi, and N. Takahashi, 2004: A dual-frequency rain profiling algorithm without the use of the surface reference technique. *IEEE Trans. Geosci. Remote Sens.,* **42,** 2214–2225.

Marzoug, M., and P. Amayenc, 1991: Improved range-profiling algorithm of rainfall rate from a spaceborne radar with path-

integrated attenuation constraint. *IEEE Trans. Geosci. Remote Sens.,* **29,** 584–592.

——, and ——, 1994: A class of single- and dual-frequency algorithms for rain-rate profiling from a spaceborne radar. Part I: Principle and tests from numerical simulations. *J. Atmos. Oceanic Technol.,* **11,** 1480–1506.

Matrosov, S. Y., K. A. Clark, B. E. Martner, and A. Tokay, 2002: X-band polarimetric radar measurements of rainfall. *J. Appl. Meteor.,* **41,** 941–952.

——, D. E. Kingsmill, B. E. Martner, and F. M. Ralph, 2005: The utility of X-band polarimetric radar for quantitative estimates of rainfall parameters. *J. Hydrometeor.,* **6,** 248–262.

Meneghini, R., J. Eckerman, and D. Atlas, 1983: Determination of rain rate from a space-borne radar using measurements of total attenuation. *IEEE Trans. Geosci. Remote Sens.,* **21,** 34–43.

——, T. Kozu, H. Kumagai, and W. C. Boncyk, 1992: A study of rain estimation methods from space using dual-wavelength radar measurements at near-nadir incidence over ocean. *J. Atmos. Oceanic Technol.,* **9,** 364–382.

Press, W. H., S. A. Teukolsky, W. T. Vetterling, and B. P. Flannery, 1992: *Numerical Recipes in FORTRAN.* 2d ed. Cambridge University Press, 933 pp.

Rose, C. R., and V. Chandrasekar, 2006: Extension of GPM dual-frequency iterative retrieval method with DSD-profile constraint. *IEEE Trans. Geosci. Remote Sens.,* **44,** 328–335.

Seifert, A., 2005: On the shape–size relation of drop size distributions in convective rain. *J. Appl. Meteor.,* **44,** 1146–1151.

Testud, J., E. Le Bouar, E. Obligis, and M. Ali-Mehenni, 2000: The rain profiling algorithm applied to polarimetric weather radar. *J. Atmos. Oceanic Technol.,* **17,** 332–356.

Ulbrich, C. W., 1983: Natural variations in the analytical form of the raindrop size distribution. *J. Climate Appl. Meteor.,* **22,** 1764–1775.

Zhang, G., J. Vivekanandan, and E. Brandes, 2001: A method for estimating rain rate and drop size distribution from polarimetric radar measurements. *IEEE Trans. Geosci. Remote Sens.,* **39,** 830–841.